Adaptive Virtual Inertia Control for Stable Microgrid Operation Including Ancillary Services Support

Filipe Perez, Gilney Damm, Cristiano Maria Verrelli, Paulo Ribeiro

Adaptive Virtual Inertia Control for Stable Microgrid Operation including Ancillary Services Support

Filipe Perez, Gilney Damm, *Member, IEEE*, Cristiano M. Verrelli, Paulo F. Ribeiro, *Fellow, IEEE*

***Abstract*—This paper proposes an adaptive virtual inertia control system for stable operation of Microgrids: it theoretically improves recent related results in the literature. The overall control system is conceived to provide ancillary services support (namely, enhanced frequency regulation with inertial response and voltage support) to an AC/DC Microgrid that consists of a DC bus providing power to the AC one, being in turn composed of a diesel generator and loads. The AC voltages and currents are controlled via a nonlinear algorithm based on control-induced time-scale separation and singular perturbation analysis, whose use greatly simplifies the control design and the choice of the tuning gains, when compared to the classical linear controls. With the aim of reducing oscillations from the grid by assuring suitable short circuit ratio and proper X/R characteristics, a virtual impedance is also implemented, along with frequency and voltage droops: they constitute high level controllers that give references to the virtual inertia scheme and compose a comprehensive control. Detailed simulations illustrate, in different relevant settings, the performance of the proposed scheme.**

***Index Terms*—Adaptive virtual inertia, nonlinear control, singular perturbation analysis, inertial support, Microgrids, power system stability.**

I. Introduction

CLASSICALLY, power systems have been based on synchronous machines rotating in synchronism, sharing power to supply loads, and providing natural inertia (frequency response) in spite of disturbances or changes in system operating conditions. Nowadays, this traditional layout is quickly changing, due to the large penetration of power electronics through renewable energy sources, energy storage units, and modern loads [1], [2], [3].

Power converters are the natural interconnection between electronic loads and Direct Current (DC) equipment in general. Large power outfits such as HVDC lines and pumped storage plants also exhibit, in this context, a power converter interface. Since power converters cannot have a natural inertial response as conventional synchronous generators, load changes and other system perturbations may lead to power oscillations and problems concerning operating margins. Lack of inertia thus becomes a relevant issue, and in some situations, frequency stability of networks with large shares of power electronics might be completely lost [4], [5], [6]. With respect to this, the black-out on August 9, 2019, in the United Kingdom [7], with its cause being verified by the reduction of the system inertia, has become a classical example for the effect of large penetration of power electronic devices connected to the electrical grid. A number of control strategies to maintain voltage and frequency stability in weak/isolated grids have been proposed in late researches. Indeed, such low-inertia power systems tend to be very sensitive to disturbances, in particular due to the power converters that replace the synchronous machines in generation units of modern power systems. The most used strategy in these cases is the *droop control*, where the physical relation of Active Power with Frequency ($P-f$) and of Reactive Power with Voltage ($Q-V$) are imposed for inductive line systems to assure a stable operation of the network. Such control technique has been widely applied enabling flexible operation of the connected distributed resources, thus making possible to share the burden of achieving frequency and voltage stability in the network. Nevertheless, classic $P-f$ and $Q-V$ droop strategies restrictively rely on the impedance characteristic of the network, only acting at steady-state, and then the lack of effects during transients makes droop control unsuitable to improve frequency stability. For this reason, some variants of droop control have been proposed to take into account transient response by inserting a frequency derivative-based term. On the other hand, droop control is applied as the primary control in an hierarchical structure, where the secondary control is designed to mitigate frequency and voltage deviation on a slower time-scale [8], [9], [10], [11].

An interesting possibility to simultaneously solve frequency, inertial, and voltage stability problems is represented by the concept of synchronverters [12], then expanded into Virtual Synchronous Machines (VSM) concept in [13], [14], [15], [16], or of VIrtual Synchronous MAchines (VISMA) in [17]. All of them are composed of power converters (Voltage Source Converter - VSC) that mimic synchronous machines. In this way, it is much easier to integrate such systems into the power network, while providing a framework that practitioners are well acquainted with [18], [19], [20]. Within this framework, the *virtual inertia approach* has raised much interest in the recent years, where the steady-state and the transient characteristics of synchronous machines are emulated by adding a swing equation-based term in order to improve inertial response. In particular, the virtual inertia concept

Filipe Perez is with CentraleSupélec, L2S Laboratory, Paris-Saclay University, Gif-Sur-Yvette, France (e-mail: filipeperez.10@gmail.com)

Gilney Damm is with LISIS Laboratory, University Gustave Eiffel, Marne-la-Vallée, France (e-mail: gilney.damm@univ-eiffel.fr)

Paulo F. Ribeiro and Filipe Perez is with ISEE, Federal University of Itajubá, Itajubá, Brazil (e-mail: pfribeiro@ieee.org)

Cristiano M. Verrelli is with the Electronic Engineering Department, University of Rome Tor Vergata, Rome, Italy (e-mail: verrelli@ing.uniroma2.it)

for distributed generation has been introduced in [19], [21], [22], while its application to grid-connected Microgrids and to isolated power systems have been presented in [23], [24] and [25], respectively. A comparison between the closed-loop performance obtained through the virtual inertia approach and the droop strategy has been performed in [26] through a small-signal stability analysis. In [16], an alternating moment of inertia has been proposed: the inertia coefficient is viewed as a controlled variable that can change according to the operational condition of the system. Its effects have been accordingly illustrated by a transient energy analysis taking into account the stability properties of the system. In [27], [28], improved frequency regulation has been reached on the basis of on adaptive virtual inertia, where the inertia constant varies according to the frequency deviation: both the inertia constant and the damping term become time-varying, such that frequency excursions are reduced and inertial response is improved. Even though such an approach is able to combine the benefits of large inertia and low inertia characteristics by considering ancillary service provision and inertial support, numerical issue arise due to the appearance of a second degree algebraic equation possessing two solutions at each time.

It is relevant to mention that in 2022, the European Network of Transmission System Operators published a paper addressing the stability of power electronics dominated systems, highlighting the frequency stability and converter-driven stability as key factors for the success of the energy transition [29]. The VSM strategy is typically implemented through a reduced-order synchronous machine model, with the active power balance being associated with the system inertia and the power angle being generated by the swing equation. The reactive power control (primary control) for voltage regulation is applied to the VSM via the droop equation, which is independent of the inertia emulation [30]. With this respect, an example of a direct implementation of VSM concept has been developed in [31], in which the voltage amplitude reference from droop control and the resulting power angle (coming from the swing equation) have been directly used to generate the Pulse Width Modulation (PWM) signals of the power converter. Despite its simple implementation, the above approach however neglects voltage and current saturation, over-current limits, and protection strategies. On the other hand, when the voltage control loop is implemented through a reactive power control including an inner current control loop, a more flexible VSM implementation is allowed, including saturated outputs, but a proper tuning of the controllers is definitely required [32], [30].

The contribution of this paper is constituted by an overall control scheme for an AC/DC Microgrid. The original key point is given by a new virtual inertia control that uses an adaptive inertia coefficient: not only it improves theoretically the one in [27], but also it enhances frequency stability, while providing inertial support to the AC side of the Microgrid. In particular, the adaptive virtual inertia scheme is defined in order to obtain a desired behavior for the inertia coefficient, while removing the occurrence of the second degree algebraic equation in [27] with its two solutions at each time. The proposed virtual inertia scheme allows for ancillary services provision to the AC side of the grid using energy from the DC side, which fits better with interconnected renewable energy sources, storage, and power electronic loads like electric vehicles. The AC Microgrid is then stabilized by a nonlinear control strategy based on a singular perturbation approach, with an explicit control-induced time-scale separation developed for voltages and currents. In particular, by following power system insights, while resorting to feedback linearization techniques and singular perturbation analysis, currents are controlled such as to behave as a fast subsystem, with the boundary layer model being constituted by the voltage dynamics (slow subsystem). A virtual impedance is also inserted to guarantee an X/R ratio similar to classical power systems, in spite of impedance variations in the considered weak Microgrid. This, in turn, assures the decoupling between active and reactive powers. Hence, $(P-f)$ and $(Q-V)$ relations can be imposed. Detailed simulations illustrate the performance of the proposed scheme compared with the droop control and the industrial standard linear control.

II. Microgrid Model and Overall Control Strategy

A. Dynamic Electrical Model

The electrical model of the AC/DC Microgrid is introduced in this section. The Microgrid consists of the following two parts: 1) the DC grid composed by a number of elements, including distributed energy sources (PV arrays), storage systems such as supercapacitors and batteries, DC loads like electric vehicles, and smart buildings. These elements are interconnected through a DC bus modeled as a capacitor (V_{dc}); 2) the three phase AC Microgrid composed of a diesel generator and a local distribution system represented here by the AC load, which contains four different loads with their impedance lines and nominal power. Loads L_1 and L_2 are modeled as Z constant and loads L_3 and L_4 are modeled as PQ constant. The impedance line is modeled to link the AC bus with the Point of Common Coupling (PCC), namely the measurement point for AC voltage. The output LC filter from the VSC interconnects the AC side with the DC side of the Microgrid[1].

The devices on the DC Microgrid are controlled via a distributed control strategy: the supercapacitor controls the DC bus voltage, hence the power flow balance in transients; the battery performs the power flow balance in long term, according to the PV dispatch and the load demand; the PV array is the main generation of the DC system and energy is extracted using a Maximum Power Point Tracking (MPPT) algorithm; the time varying DC load is properly supplied. For the sake of clarity, the electrical model of the AC/DC Microgrid is depicted in Fig. 1.

On the other hand, the DC bus constitutes the interconnection point of the Microgrid devices, represented by the capacitor C_{dc}. The voltage dynamics on the DC bus are accordingly written as:

$$\dot{V}_{dc} = \frac{1}{C_{dc}}[I_{sc} + I_{bt} + I_{pv} - I_{dc} - I_{ac}], \qquad (1)$$

[1]The adaptive inertia scheme will be actually applied to this VSC, resulting in a VSM.

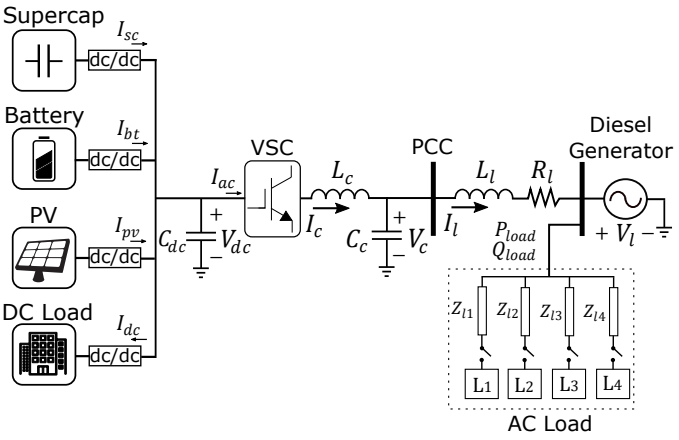

Fig. 1. Proposed AC/DC Microgrid, in which the VSC interconnects the DC grid with the diesel generator- based AC grid.

where I_{sc} is the current in the supercapacitor, I_{bt} is the current in the battery, I_{pv} is the current from the PV generation, I_{dc} is the DC Load current demand and I_{ac} is the current flowing to the AC side of the Microgrid. Consequently, the DC bus voltage indicates the balance of power in the whole DC grid. For the sake of brevity, the DC grid will not be further detailed and it will be only represented by this lumped model. More detailed models of each subsystem can be found in [33].

The VSC has an LC filter, represented by L_c and C_c, connected to the PCC of the AC Microgrid. The line impedance is represented by L_l and the active losses rely on R_l. The state-space model for the AC side of the system is thus introduced as follows:

$$\dot{V}_{c,d} = \frac{I_{c,d}}{C_c} - \frac{I_{l,d}}{C_c} + \omega_{vsm} V_{c,q} \tag{2}$$

$$\dot{V}_{c,q} = \frac{I_{c,q}}{C_c} - \frac{I_{l,q}}{C_c} - \omega_{vsm} V_{c,d} \tag{3}$$

$$\dot{I}_{c,d} = -\frac{R_c}{L_c} I_{c,d} + \omega_{vsm} I_{c,q} + \frac{1}{2L_c} V_{dc} m_d - \frac{V_{c,d}}{L_c} \tag{4}$$

$$\dot{I}_{c,q} = -\frac{R_c}{L_c} I_{c,q} - \omega_{vsm} I_{c,d} + \frac{1}{2L_c} V_{dc} m_q - \frac{V_{c,q}}{L_c} \tag{5}$$

$$\dot{I}_{l,d} = -\frac{R_l}{L_l} I_{l,d} + \omega_{vsm} I_{l,q} + \frac{V_{c,d}}{L_l} - \frac{V_{l,d}}{L_l} \tag{6}$$

$$\dot{I}_{l,q} = -\frac{R_l}{L_l} I_{l,q} - \omega_{vsm} I_{l,d} + \frac{V_{c,q}}{L_l} - \frac{V_{l,q}}{L_l}. \tag{7}$$

It is expressed in synchronous reference frame according to the Park transformation. In particular, $V_{c,d}$ and $V_{c,q}$ are the voltages on the LC filter capacitor C_c; $I_{c,d}$ and $I_{c,q}$ are the currents on the LC filter inductor L_c; $I_{l,d}$ and $I_{l,q}$ are the line currents; $V_{l,d}$ and $V_{l,q}$ are the voltages on the diesel generator; ω_{vsm} is the VSM frequency. Finally, the VSC modulation indexes are m_d and m_q, which constitute the control inputs.

B. Control Scheme Structure

The hierarchical control scheme proposed in this paper, whose specific control actions will be detailed in the next sections (with the original contribution of this paper, as aforementioned, being represented by the adaptive virtual inertia scheme of Section IV.A), is reported in Fig. 2. It includes the active and reactive power control given by the droop controllers.

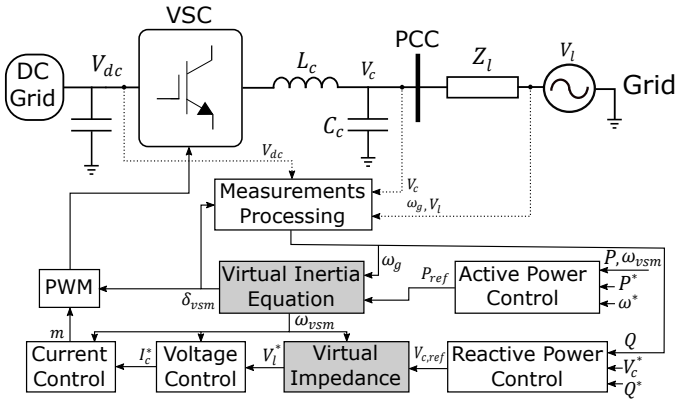

Fig. 2. Proposed adaptive virtual inertia scheme and nonlinear voltage control using virtual impedance.

The active power droop provides the references for the swing equation generating dynamically the power angle of the VSC. The reactive power droop provides voltage and reactive power references, with a virtual impedance being inserted into the voltage reference to improve the damping, the power sharing, and the decoupling of active and reactive power flows. The local control laws, which are applied to the real actuators represented by the power converter PWM, are in turn designed on the basis of a control-induced time-scale separation for voltages and currents. On the other hand, for what the DC part of the Microgrid is concerned, the nonlinear control strategy of [33] is adopted to keep the DC bus voltage inside a tight operation region, obtaining Input-to-State Stability (ISS) property: the power flow balance is assured. In other words, the Microgrid DC bus is assumed to be able to provide power to the AC Microgrid and it is thus here represented by a DC power source [34], [35], [36].

Remark 1. *It is current practice in power systems of all sizes (in transmission and distribution grids) to aggregate power generators, following a Center of Inertia procedure, into a single machine that represents the behavior of the full system. In this paper, the case of a stable Microgrid is addressed, where the power converter is supporting the grid (ancillary services) but is not solely responsible for its stability. The ubiquitous nature of frequency makes this model well capture all the relevant aspects of dynamics concerning frequency and angle stability.*

III. Primary Control

The primary control (higher level controller) provides standard ancillary services to the AC grid. In particular, the primary control generates the references to be followed by the lower level controllers: it is a higher level controller that acts in a much slower time frame (several seconds) than the lower level ones (tens to hundred of milliseconds), relying instead on steady-state power system considerations.

A. Active and reactive power control

The active power reference is computed, on a slower time-scale, by an active power-frequency droop strategy. Such a

reference will be treated as a constant when included in the subsequent swing equation (12). According to such a strategy, the active power reference obeys the reverse droop relationship [37]:

$$P_{ref} = P^* - K_\omega[\omega_{vsm} - \omega^*], \tag{8}$$

where: P^* is the desired active power to be injected/absorbed into the grid, derived by assuming a tertiary controller for power dispatch schedule; K_ω is the $P-f$ droop gain; ω^* is the angular speed reference, i.e., $\omega^* = \omega_o$ with ω_o being the nominal grid frequency; ω_{vsm} is the angular speed, from which the VSM phase angle δ_{vsm} of Fig. 2 is derived by integration.

The voltage reference $V_{c,d_{ref}}$, used by the converter voltage control for $V_{c,d}$, is computed by means of a reactive power-voltage droop strategy, where the voltage is controlled at the PCC (LC filter voltage on capacitor C_c) [38]. It is thus given by:

$$V_{c,d_{ref}} = V_{c,d_{ref}}^* - K_q[Q - Q^*], \tag{9}$$

where the notation $V_{c,d}$ classically refers to the voltage amplitude, with $V_{c,d_{ref}}^* = 1$ p.u. and $V_{c,q_{ref}}^* = 0$ being the desired voltages from synchronous reference frame adoption; Q^* is the desired reactive power injected/absorbed into the grid from a tertiary controller; K_q is the droop gain for reactive power.

Remark 2. *Equations (8) and (9) are known as the droop references for the active power and the voltage, respectively. The droop coefficients K_ω and K_q are typically computed on the basis of the maximum and minimum modulus of the allowed frequency and voltage amplitude, combined with the power capacity of the VSC [39].*

B. Virtual impedance

Microgrids usually have reduced impedance characteristics and those ones can vary according to the system operating condition in response to load changes. A virtual impedance is thus imposed to ensure the desired characteristics of short circuit and X/R ratio, while avoiding several electric issues of weak grids [40], [41]. As a consequence, the voltage amplitude reference from the droop equation (9) is summed with the virtual impedance, that is represented by a virtual resistance (R_v) and a virtual inductance (L_v). In other words, the voltage reference including the virtual impedance reads:

$$V_{c,d}^* = V_{c,d_{ref}} - R_v I_{l,d} + \omega_{vsm} L_v I_{l,q} \tag{10}$$

$$V_{c,q}^* = -R_v I_{l,q} - \omega_{vsm} L_v I_{l,d}, \tag{11}$$

where $V_{c,d_{ref}}$ is the voltage reference from the droop controller in (9) and $V_{c,q_{ref}} = 0$.

Remark 3. *The insertion of the virtual impedance is not only used to diminish the oscillations that are commonly present in Microgrids due to their low impedance values, but it is also used to modify the dynamics and the steady-state features of the VSM. The displacement of the phase angle between the voltage (V_l) and the converter output voltage (V_c) caused by the virtual power flow, allows the VSM to improve voltage control in the converter. It also reduces the sensitivity to disturbances in the grid and emulates the synchronous impedance quasi-stationary characteristics of synchronous generators [42], [43], [44].*

Remark 4. *The X/R and Short Circuit Ratio (SCR) are standard parameters of power systems. The virtual impedance allows for imposing the feature of strong grids in weak grids, which means that the SCR and the X/R ratio can be controlled to improve the system stability. Therefore, suitable values for SCR and X/R result in some advantages: the decoupling effect of Active and Reactive power is obtained by increasing the X/R ratio to obtain an inductive line (as traditional transmission lines), which is important in light of the standard references for active and reactive powers coming from the Transmission System Operator; increased X/R ratio improves the operation range for the reactive power control of the converter (reactive power support capacity), and, as a consequence, the voltage support is also improved; the X/R value can also change the capacitance feature of the line to improve power transfer and power factor.*

IV. Local Controls

This section includes the original contribution of this paper. It presents the lower level controllers, named local controls, which consist of the virtual inertia scheme along with the voltage and current control loops reported in Fig. 2. They evolve in a much faster time scale than the references provided by the higher level controllers. Therefore, the references from primary control will be taken as constant in the local control time-frame depicted here.

A. Adaptive virtual inertia scheme

The VSM scheme will mimic a synchronous machine, whose frequency dynamics is represented by the active power balance and damping factor:

$$\dot{\tilde{\omega}} = \frac{1}{H}[P_{ref} - P - D_p\tilde{\omega}], \tag{12}$$

with $\tilde{\omega} = \omega_{vsm} - \omega_g$ being the frequency deviation, ω_g being the angular speed of synchronous machine (grid), H being the virtual inertia coefficient and D_p being the damping factor. As aforementioned, P_{ref} is the active power droop reference (8) and P is the AC grid measured power. In this case, $P = P_{\max}\sin\delta$, with $P_{\max}$ being the maximum dispatchable power in the converter and δ being the power angle[2].

The swing equation of the proposed virtual inertia can be thus rewritten as a function of the power angle δ, remarking that: $\dot{\delta} = \omega_{vsm} - \omega_g$. Equation (12) thus becomes (see [45]):

$$H\ddot{\delta} = P_{ref} - P_{\max}\sin(\delta) - D_p\dot{\delta}. \tag{13}$$

Originally, the inertia coefficient is constant, adapted from [46] as:

$$H_o = \frac{J\omega_o^2}{2\mathrm{S}_{VSC}}, \tag{14}$$

[2]The maximum available power is given by $P_{\max} = EV_c/X_{eq}$ when $\delta = \pi/2$, with E being the output voltage on VSC, V_c being the PCC voltage and X_{eq} being the system equivalent reactance.

where S_{VSC} is the nominal apparent power of the converter and J is the emulated moment of inertia.

Remark 5. *The virtual inertia coefficient is properly chosen to avoid power oscillations and poor frequency response. The common procedure to shape the power angle dynamic profile resorts to the approximation*[3] *of (13) involving the second order transfer function [46], [47]:*

$$\frac{\mathcal{L}[\delta](s)}{\mathcal{L}[P_{ref}](s)} = \frac{1}{Hs^2 + D_p s + P_{\max}}, \tag{15}$$

with natural frequency $\omega_n = \sqrt{P_{\max}/H}$ *and damping ratio* $\zeta = D_p/2H\omega_n$*. The inertia* H *is then tuned by setting* ζ *according to the desired transient response and by picking the damping term through the same procedure at the root of the choice for the droop coefficients (yielding* $D_p \geq K_\omega$*)*[4].

Now, the larger the inertia coefficient is, the smaller the frequency deviation is and the longer the settling time results, whereas a smaller inertia coefficient implies a higher frequency deviation and a shorter settling time. The inertia coefficient is thus the key for inertial support and frequency regulation in the ancillary services provision context, since it indicates the amount of energy that can be stored in the rotating mass of synchronous machines. In other words, a larger inertia coefficient allows for large disturbances without large frequency deviations, whereas, when the coefficient of inertia is relatively small, the frequency is more susceptible to deviations, easily moving from its nominal operation point in response to disturbances.

Moving along the direction of adjusting the inertia, the inertia emulated in power converters can be accordingly treated as time varying, which can act to supply ancillary services stabilizing the operation of the system [27], [48], [16]. The inertia is therefore not fixed according to the rotating mass value, but it varies in a smart way according to the frequency behavior. It is aimed to reduce frequency deviation when frequency moves from an equilibrium point (increased inertia) and to reduce settling time when frequency approaches the new equilibrium point (decreased inertia). To the same purpose, the following variable inertia coefficient:

$$H = H_o + K_M(\omega_g - \omega^*)\dot{\omega}_g \tag{16}$$

has been proposed in [27]. It provides a good behavior for inertia coefficient during transients, but generates numerical issues when applied to (12), leading to a second degree algebraic equation that possesses two solutions at each time.

The original version of the time-varying inertia coefficient, which imposes the desired inertia behavior (while removing the occurrence of the aforementioned second degree algebraic equation), is here designed as:

$$\begin{aligned} H &\triangleq \mathrm{sat}_{(H_{\min},H_{\max})}(\xi) \\ \xi &\triangleq H_o + \frac{K_M\tilde{\omega}}{H_o}[P_{ref} - P_{\max}\sin\delta - D_p\tilde{\omega}], \end{aligned} \tag{17}$$

where H_o is given by (14) or chosen to impose the desired transient response at steady-state to the second order differential equation (13); $\mathrm{sat}_{(H_{\min},H_{\max})}(\xi)$ is the continuous saturation function that is linear for $\xi \in [H_{\min}, H_{\max}]$, with $H_{\min}$ and $H_{\max}$ suitable positive constants satisfying $H_{\min} \leq H_o \leq H_{\max}$; K_M is the positive gain that sets the amount of inertia coefficient variation. Such an amount directly affects frequency deviations and the Rate of Change of Frequency (RoCoF). It assures the desired behavior for the electric grid.

Define $\Phi = P_{ref} - P_{\max}\sin(\delta) - D_p\tilde{\omega}$ in (12) and rewrite the second equation of (17) as

$$\xi \triangleq H_o + \frac{K_M\tilde{\omega}\Phi}{H_o}. \tag{18}$$

When the proposed inertia coefficient (17) is substituted into the swing equation (12), the resulting virtual swing equation can be expressed as:

$$\dot{\tilde{\omega}} = \frac{H_o\Phi}{H_o^2 + K_M\tilde{\omega}\Phi}, \tag{19}$$

for ξ lying into the saturation bounds $H_{\min}, H_{\max}$. Then, considering outer bounds, it results:

$$\dot{\tilde{\omega}} = \frac{\Phi}{H_{\min}} = \frac{\Phi}{H_o} + \Phi\left[\frac{1}{H_{\min}} - \frac{1}{H_o}\right], \tag{20}$$

for $\xi < H_{\min}$ and it results in the following:

$$\dot{\tilde{\omega}} = \frac{\Phi}{H_{\max}} = \frac{\Phi}{H_o} + \Phi\left[\frac{1}{H_{\max}} - \frac{1}{H_o}\right], \tag{21}$$

for $\xi > H_{\max}$.

Stability analysis. The appearance of H within $\dot{\omega}_g$ of (16) (that leads to the aforementioned second degree algebraic equation) is removed by the use of H_o in the second term of the right hand side of the second equation in (17). Nevertheless, the following theorem illustrates how the adaptive virtual inertia mechanism (17) guarantees stability properties that enrich the ones owned by the system with constant inertia. In particular, the same Lyapunov function (time t dependence is hereafter omitted):

$$W_\omega = \frac{1}{2}H_o\tilde{\omega}^2 - P_{ref}(\delta - \bar{\delta}) - P_{\max}(\cos\delta - \cos\bar{\delta}) \tag{22}$$

of [49] (see also [46]) can be used to assess such properties.

Theorem IV.1. *Let* $\bar{\delta} \in (-\pi/2, \pi/2)$ *satisfy* $P_{ref} = P_{\max}\sin(\bar{\delta})$*. Then the adaptive inertia coefficient (17) assures,* via *(22), local asymptotic stability of the equilibrium point* $(\delta - \bar{\delta}, \tilde{\omega}) = 0$ *for the system* $(\delta - \bar{\delta}, \tilde{\omega})$*, consisting of* $\dot{\delta} = \tilde{\omega}$ *and (12). In addition, when* $H_{\min}$ *and* $H_{\max}$ *collapse into* H_o*, or conversely* K_M *is set to zero, the classical stability result for fixed inertia is recovered.*

[3]Since, in general, the swing equation operating points belong its linear region, i.e., the $P - \delta$ curve is limited to the nominal operating region of the generator, the nominal power of the generator is given for small values of the power angle and thus the linearization holds true. This means that linear dynamics dominate over nonlinear dynamics in the typical operating region.

[4]Nevertheless, the VSM parameters can be obtained from the real values of synchronous machines, since originally they represented the physical values of the equipment.

Proof. Now consider the equilibrium point ($\delta = \bar{\delta}$, $\tilde{\omega} = 0$) for the system ($\bar{\delta}$ is the equilibrium point for the power angle, such that the power reference supply is attained) and take the time-derivative of (22) along the trajectories of the closed loop system as:

$$\dot{W}_\omega = \tilde{\omega} H_o \dot{\tilde{\omega}} - P_{ref}\tilde{\omega} + P_{\max}\tilde{\omega}\sin\delta. \tag{23}$$

By exploiting the definition of Φ with equations (19) and (12), while viewing H as a function of time within the positive bounds $H_{\min}$, $H_{\max}$, write:

$$H_o\Phi = H_o^2\dot{\tilde{\omega}} + K_M\tilde{\omega}\frac{\Phi^2}{H}, \tag{24}$$

which leads to:

$$H_o\dot{\tilde{\omega}} = -\left[D_p + \frac{K_M}{H_o H}\Phi^2\right]\tilde{\omega} + P_{ref} - P_{\max}\sin\delta, \tag{25}$$

so that (23), when ξ lies within saturation bounds, reads:

$$\begin{aligned}\dot{W}_\omega = (P_{ref} - P_{\max}\sin\delta)\tilde{\omega} - \left[D_p + \tfrac{K_M}{H_o H}\Phi^2\right]\tilde{\omega}^2 + \\ -(P_{ref} - P_{\max}\sin\delta)\tilde{\omega},\end{aligned} \tag{26}$$

resulting in:

$$\dot{W}_\omega \;=\; -\left[D_p + \frac{K_M}{H_o H}\Phi^2\right]\tilde{\omega}^2. \tag{27}$$

Now, by virtue of (20) and (21), (23) reduces to:

$$\dot{W}_\omega = -D_p\tilde{\omega}^2 + \left[\frac{H_o}{H_{\min}} - 1\right]\Phi\tilde{\omega} \tag{28}$$

when $\xi < H_{\min}$ and thus $\Phi\tilde{\omega} < 0$ from (18), whereas it reduces to:

$$\dot{W}_\omega = -D_p\tilde{\omega}^2 + \left[\frac{H_o}{H_{\max}} - 1\right]\Phi\tilde{\omega} \tag{29}$$

when $\xi > H_{\max}$ and thus $\Phi\tilde{\omega} > 0$ from (18). In summary, for any $t \geq 0$, we conservatively get:

$$\dot{W}_\omega(t) \leq -D_p\tilde{\omega}^2(t), \tag{30}$$

where the enforced equations (27), (28), (29) including the additional $\Phi\tilde{\omega}$ terms hold true. Now, set $\mathcal{P} = -P_{ref}(\delta - \bar{\delta}) - P_{\max}(\cos\delta - \cos\bar{\delta})$ and write:

$$\mathcal{P} \;=\; -P_{\max}(\sin\bar{\delta} - \sin\xi_\delta)(\delta - \bar{\delta}), \tag{31}$$

where ξ_δ, according to the mean value theorem, belongs to the set $(\delta, \bar{\delta})$. Therefore, W_ω is a $\mathcal{C}^1$ function being positive definite on a neighborhood $\mathcal{S}$ of the origin (namely, $W_\omega(0) = 0$ and $W_\omega(s) > 0$ for any $s \in \mathcal{S} \setminus \{0\}$), whereas the system $(\delta - \bar{\delta}, \tilde{\omega})$ is in the form $\dot{x} = f(x)$, with $f(0) = 0$. Consequently, according to the LaSalle-Krasovskii stability criterion, the origin is a local asymptotically stable equilibrium point for the system. Finally, when $H_{\max} - H_{\min}$ shrinks and both $H_{\min}$ and $H_{\max}$ converge to H_o (with K_M being zero), then:

$$\dot{W}_\omega(t) = -D_p\tilde{\omega}^2(t), \tag{32}$$

so that the case of constant inertia is trivially recovered. □

The proof of the previous theorem shows, through (27), (28), (29), that (17) improves the frequency support: it is effective to reduce frequency variations and to enhance the frequency Nadir. In particular:

- *Large inertia.* For $\tilde{\omega} > 0$ and $\dot{\tilde{\omega}} > 0$ or $\tilde{\omega} < 0$ and $\dot{\tilde{\omega}} < 0$, indicates frequency acceleration, the angular speed is deviating from its original value; therefore, the inertia increases to avoid frequency deviation.
- *Small inertia.* For $\tilde{\omega} < 0$ and $\dot{\tilde{\omega}} > 0$ or $\tilde{\omega} > 0$ and $\dot{\tilde{\omega}} < 0$, indicates frequency deceleration, the angular speed is moving towards the right direction to possibly reach its steady-state value; therefore, the inertia decreases to make the frequency deviation return faster at zero.

The idea underlying the adaptive virtual inertia control leads to improve the inertia response and to provide frequency support. These are related to ancillary services provision, which does not exclusively imply a faster frequency response. With respect to frequency response requirements, the frequency nadir and RoCoF are the real priorities to improve the system stability. Therefore reducing RoCoF and frequency nadir may slower the frequency dynamics to reduce overshoots and oscillations. Also, the slower frequency excursions are less likely to trigger system protections, which further improves the operation of the system. On the other hand, increasing the frequency dynamics at a proper time allows for a smoother frequency accommodation, without oscillations.

Remark 6. *Parameter K_M and bounds $H_{\min}, H_{\max}$ can be set in practice by considering, for instance, the following (conservative) chain of inequalities:*

$$H_{\min} \leq H_o \pm \frac{K_M}{H_o}\tilde{\omega}_{\max}\Phi_{\max} \leq H_{\max} \tag{33}$$

where $\tilde{\omega}_{\max}$ is the maximum modulus of the allowed frequency deviation and $\Phi_{\max} = P_{\max}\tilde{\delta}_{\max} + D_p\tilde{\omega}_{\max}$ ($\tilde{\delta}_{\max}$ is the maximum modulus of the allowed power angle deviation from $\bar{\delta}$). Therefore, parameter K_M obeys:

$$0 < K_M \leq \max\left\{\frac{(H_o - H_{\min})H_o}{\tilde{\omega}_{\max}\Phi_{\max}}, \frac{(H_{\max} - H_o)H_o}{\tilde{\omega}_{\max}\Phi_{\max}}\right\} \tag{34}$$

In other words, the limits for the adaptive inertia coefficient (H) are given according to the grid requirements. Indeed, these values are calculated in practice according to the established rate of change of frequency (RoCoF), the frequency nadir and the frequency accommodation time (parameters defined in the grid-code). In this case, the lower limit for the inertia ($H_{\min}$) is mainly given by the maximum allowed nadir ($\tilde{\omega}_{\max}$): since small inertia values tend to have higher frequency overshoots, the only absolute constraint is $H_{\min} > 0$ (where $H_{\min} = 0$ would result in a singularity). Even for the upper limit of the inertia ($H_{\max}$), the greatest influence is on the limit for frequency accommodation time, since high inertia values tend to have slower dynamics. Therefore, K_M parameter can be set in such a way as to fit inequality (33). The inequalities (33) and (34) provide the parameter bounds for K_M, which is the last parameter to be tuned.

Remark 7. *The synchronism between the diesel generator and the VSC is created by the virtual swing equation, similar to*

the physical behavior of conventional synchronous machines in parallel, where a Phase-Looked Loop (PLL) is not necessary. However, PLL is still used for frequency measurement.

Remark 8. *The stand-alone operation can be achieved from virtual inertia control by removing the power references in (8) and (9), where the frequency and voltage regulation is directly resulted from power balance of the system. Therefore, the VSC is able to supply the microgrid in grid-forming operation, considering a generator failure.*

B. Voltage and current control

The voltage and current controllers are here designed via a control induced time-scale separation (see [50], [51], [52]) to artificially make the dynamics of the currents much faster than the dynamics of voltages, thus creating a singular perturbation condition. The related feedback linearization and singular perturbation steps are just sketched in this subsection, for the sake of compactness. In particular, once the references $V_{c,d}^*$ and $V_{c,q}^*$ for the voltages have been designed as in (10)-(11), the dq currents references $I_{c,d}^*$ and $I_{c,q}^*$ are used in the $V_{c,d}$ and $V_{c,q}$ equations as virtual control inputs, such to stabilize voltages $V_{c,d}$ and $V_{c,q}$ towards their references $V_{c,d}^*$ and $V_{c,q}^*$. They explicitly read:

$$
\begin{aligned}
I_{c,d}^* &= C_c\varphi_{vd} + I_{l,d} - \omega_{vsm}C_cV_{c,q} && (35)\\
I_{c,q}^* &= C_c\varphi_{vq} + I_{l,q} + \omega_{vsm}C_cV_{c,d} && (36)\\
\varphi_{vd} &= -K_{vd}(V_{c,d} - V_{c,d}^*) - K_{vd}^{\alpha}\alpha_{vd} && (37)\\
\dot{\alpha}_{vd} &= V_{c,d} - V_{c,d}^* && (38)\\
\varphi_{vq} &= -K_{vq}(V_{c,q} - V_{c,q}^*) - K_{vq}^{\alpha}\alpha_{vq} && (39)\\
\dot{\alpha}_{vq} &= V_{c,q} - V_{c,q}^*, && (40)
\end{aligned}
$$

with $K_{vd,q}$ and $K_{vd,q}^{\alpha}$ being positive gains such that the explicit time-scale separation is ensured, and $\alpha_{v,dq}$ being integral terms used to compensate for steady-state constant disturbances. The boundary layer model of the voltage dynamics is obtained by injecting the current references (35)-(40) into (2)-(3), where from singular perturbation theory, $I_{c,dq}$ are replaced by $I_{c,dq}^*$, namely:

$$\dot{V}_{c,d} = \frac{I_{c,d}^*}{C_c} - \frac{I_{l,d}}{C_c} + \omega_{vsm}V_{c,q} \quad (41)$$

$$\dot{V}_{c,q} = \frac{I_{c,q}^*}{C_c} - \frac{I_{l,q}}{C_c} - \omega_{vsm}V_{c,d}. \quad (42)$$

By applying the feedback linearization technique to the inner subsystem, the control inputs $m_{d,q}$ are designed as:

$$m_d = \tfrac{2}{V_{dc}}[L_c\varphi_{id} + R_cI_{c,d} - \omega_{vsm}L_cI_{c,q} + V_{c,d}] \quad (43)$$

$$m_q = \tfrac{2}{V_{dc}}[L_c\varphi_{iq} + R_cI_{c,q} + \omega_{vsm}L_cI_{c,d} + V_{c,q}] \quad (44)$$

with:

$$
\begin{aligned}
\varphi_{id} &= -K_{id}(I_{c,d} - I_{c,d}^*) && (45)\\
\varphi_{iq} &= -K_{iq}(I_{c,q} - I_{c,q}^*), && (46)
\end{aligned}
$$

where the gains $K_{id,q}$ are positive constants, computed by pole placement to regulate the convergence of the currents, again assuring explicit time-scale separation of voltage and current subsystems [53], [54].

TABLE I
AC MICROGRID PARAMETERS

VSC	$S_{vsm} = 1$MVA	$f_s = 25$kHz	$V_{vsm} = 400$V
LC Filter	$R_c = 20$mΩ	$L_c = 0.5$mH	$C_c = 100\mu$F
VSM	$K_w = 20$	$D_p = 50$	$H_o = 2$s
AC grid	$R_l = 0.1$mΩ	$L_l = 0.01$mH	$V_l = 400$V

Considering the current subsystem (4)-(5) subject to the control input (43)-(46) along with the voltage subsystem (2)-(3) subject to the virtual control signals (35)-(40), the closed-loop dynamics of the system can be explicitly derived. Now defining the voltage and current errors as $\tilde{V}_{c,d} = V_{c,d} - V_{c,d}^*$, $\tilde{V}_{c,q} = V_{c,q} - V_{c,q}^*$ and $\tilde{I}_{c,d} = I_{c,d} - I_{c,d}^*$, $\tilde{I}_{c,q} = I_{c,q} - I_{c,q}^*$ and taking $K_{i,d} = K_{i,q} = 1/\epsilon$, one may rewrite the closed-loop system in the standard singular perturbation form. With the currents $I_{l,d}$ and $I_{l,q}$ in (6)-(7) obeying stable dynamics and being attracted by equilibrium values that depend on the reference values $V_{c,d}^*$, $V_{c,q}^*$ and ω^* (provided by the higher level controller) and the grid parameters $V_{l,d}, V_{l,q}, L_l$ and R_l. Then, according to the singular perturbation analysis [55], any sufficiently small ϵ guarantees that the origin of the subsystem (2)-(3) is exponentially stable.

Remark 9. *The two time-scales generate a cascaded behavior for the voltage and current. This is a classical empirical approach, typically used in industry. In addition, as shown in [56], the system convergence is assured by only including a high-gain proportional controller in the lower subsystem, without resorting to the use of additional integral terms in that channel. Anyway, the corresponding integral term can be added as in the traditional power system procedures.*

V. SIMULATION RESULTS

The electrical model of the Microgrid described in Fig. 1 is implemented on *Simscape Electrical* toolbox from *Simulink*. The AC Microgrid is composed of a diesel generator and a local distribution system with four different loads, where a VSC interconnects the DC Microgrid (composed of loads, renewables and storage systems) with the AC side of the grid.

The diesel generator has a Governor to control the frequency and active power, where the control parameters are: regulator gain $K = 150$ and time constant $T_{reg} = 0.1$s, actuator time constant $T_{act} = 0.25$s and engine time delay $T_d = 0.024s$. The Automatic Voltage Regulator (AVR) is implemented to control the voltage and the reactive power from the machine excitation system [57]. The AVR parameters are: voltage regulator gain $K_{va} = 400$, time constant $T_{va} = 0.02$s and low-pass filter time constant $T_r = 0.02$s. The parameters of the AC Microgrid are introduced in Table I. The nominal frequency of the grid is $f_n = 50$Hz and the nominal power of the diesel generator is $S_{diesel} = 2$MVA with $V_l = 400$V rms nominal voltage, 2 pairs of poles and inertia coefficient of $H_{diesel} = 3$s. The Q-V droop coefficient is $K_q = 0.2$. The gains of the inner voltage and current control loops are described in Table II. Parameters of DC Microgrid are detailed in [33].

The nominal power of the VSM is $S_{vsm} = 1$MVA with nominal rms voltage of $V_{vsm} = 400$V, which are the base values for per unit transformation. Active power (P) and

TABLE II
PARAMETERS OF VOLTAGE AND CURRENT CONTROL LOOPS.

Voltage loop	$K_{v,dq} = 1/L_c$	$K^{\alpha}_{v,dq} = 10/L_c$
Current loop	$K_{id} = 500/L_c$	$K_{iq} = 500/L_c$

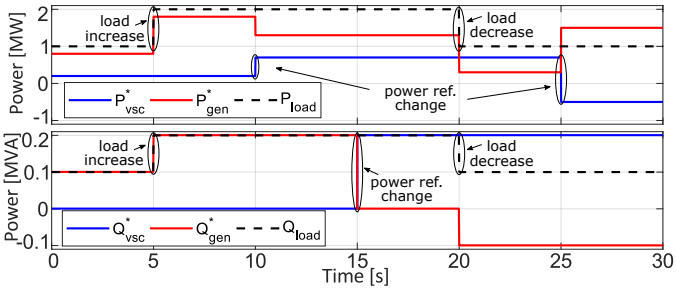

Fig. 3. The power events in the Microgrid.

reactive power (Q) injected by the VSC are controlled to their references (P^* and Q^*), given by a higher control level, assuming a power dispatch schedule (tertiary control). These references are bounded according to the capability curve of the power converter given as: $P^2 + Q^2 \leq S^2_{vsm}$. Initially, the total load demand is 1MW and 0.1MVA, where the VSC supplies 0.2MW and 0MVA, and the diesel generator complements the power supply. Therefore, a large load increase of 1MW and 0.1MVA occurs after 5 seconds of simulation (load growth in the same level of the rated power of the VSC). Within 10 seconds of simulation, the active power reference of the VSC changes to 0.7MW and within 15 seconds the reactive power reference changes to 0.2MVA. Then, within 20 seconds a load reduction of 1MW and 0.1MVA takes place and finally within 25 seconds the active power reference in the VSM changes to -0.5MW (a strong event to emphasize performance of the proposed control). The power reference of the synchronous generator and the VSC and the load demand are depicted in Fig. 3.

The controlled active and reactive powers of the VSM are presented in Fig. 4. Active power is properly controlled, following the reference with some overshoots and fast convergence during the load changes, and with smooth transients without overshoots during power reference changes. The reactive power is controlled to track its reference with stronger overshoots during load shifts and changes in power reference. This is because the droop controller is also following a voltage reference, which is given by the voltage control loop. Therefore, reactive power presents a steady-state error such as to participate in the voltage regulation besides the power balance. The reactive power flow mismatch can then be solved by a tertiary controller to provide new values for reactive power. Even with this imbalance, the reactive power is duly controlled.

The active and reactive powers supplied by the diesel generator are depicted in Fig. 5, where the power varies to stabilize the frequency following the machine governor, such that the power balance is assured and steady-state error in frequency is removed. Voltage and machine excitation are regulated by the AVR control, assuring reactive power balance at steady-state, as well as the voltage profile. The figure shows that the power response of the synchronous machine is slower

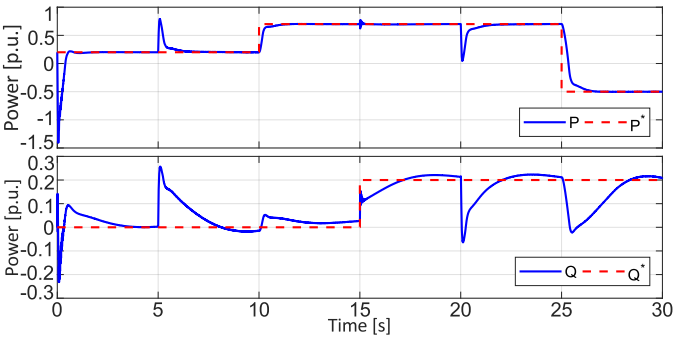

Fig. 4. The controlled active and reactive powers in the VSC of the Microgrid.

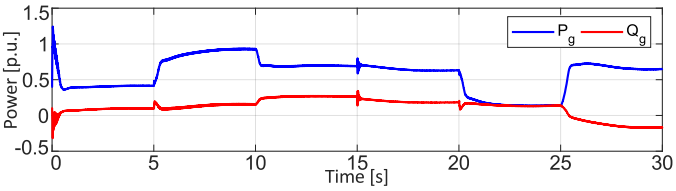

Fig. 5. The controlled active and reactive powers in the diesel generator to allow power balance.

than the power response of the VSM, since they present different parameters. The per unit base for the diesel generator is $S_b = 2$MVA.

The voltage profile on the PCC is depicted in Fig. 6, where voltage $V_{c,d}$ shows the voltage amplitude in the PCC and the quadrature voltage $V_{c,q}$ is set to zero from the synchronous reference frame. The reference $V^*_{c,d}$ is given by the droop control according to a reactive power reference in combination with the virtual impedance term. The virtual impedance is inserted to improve the controllability of the voltage, to increase the operation margins of the system and to improve stability, and also to decouple active and reactive powers, resulting in a suitable X/R ratio as traditional power systems. The voltages are properly controlled with fast transient response and very small overshoots, which results in a good voltage profile.

The steady-state errors are caused by the droop scheme, also controlling the reactive power to the given reference. An integral term can be inserted in the droop equations (8)-(9) to eliminate the steady-state errors in active and reactive powers respectively, which is a suitable application also for stand-alone operation (considering only the power converter supplying the network).

The direct and quadrature currents are presented in Fig. 7. They present a faster convergence response compared with the voltage dynamics, owing to the explicit time-scale separation induced by the nonlinear controller. The current references are given to make the voltage $V_{c,d}$ and $V_{c,q}$ be controlled to the desired references according to the singular perturbation analysis.

The frequency of the Microgrid is presented in Fig. 8, where the proposed adaptive virtual inertia is used to reduce frequency deviation and to improve frequency RoCoF, providing a better inertial support. Transients are responses to load variations (within 5 and 20 seconds of simulation time) and power reference changes (within 10, 15 and 25 seconds). As expected, the bigger the power change is, the larger the

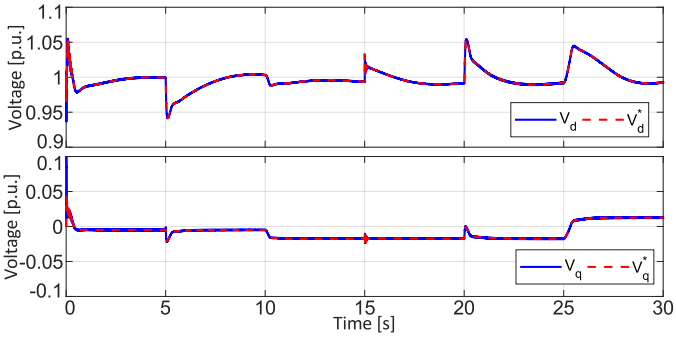

Fig. 6. The controlled voltage of the grid in the PCC.

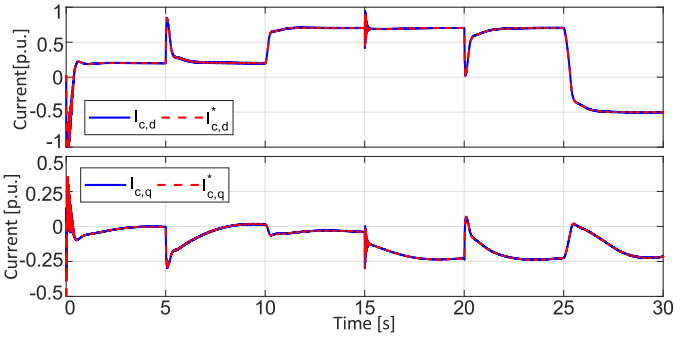

Fig. 7. The controlled currents of the VSC converter.

frequency excursion in the grid results: the last power variation in the grid, which represents a huge power variation of $1p.u.$ in the VSM, causes an overshoot of 0.5% in frequency response. The droop control developed in the VSC would result in steady-state error in frequency, but the governor of the diesel generator manages to eliminate the steady-state error, bringing the power balance to the grid.

The main idea of the adaptive virtual inertia is to have an inertia coefficient H that varies according to frequency deviation $\tilde{\omega}$ and angular acceleration $\dot{\tilde{\omega}}$. Therefore, when VSM is accelerating, the inertia increases to minimize frequency deviation and, when VSM is decelerating, the inertia decreases to speed-up reaching steady-state. The behavior of the adaptive inertia coefficient can be seen in Fig. 9. The transient behavior of the inertia is a consequence of the $\dot{\tilde{\omega}}$ and $\tilde{\omega}$ profiles, as shown in Fig. 10, where the transients are highlighted to understand RoCoF and frequency Nadir.

A. Parameters variation

To better understand the effect of parameters tuning in the adaptive virtual inertia application, a few changes in the VSM parameters are performed. In this case, the response

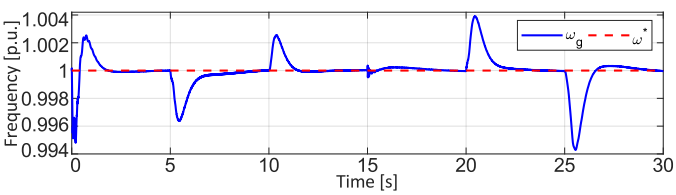

Fig. 8. Frequency of the grid and its reference.

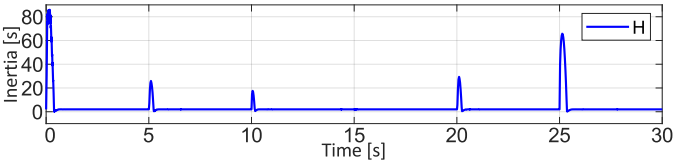

Fig. 9. Inertia coefficient behavior varying during frequency transients.

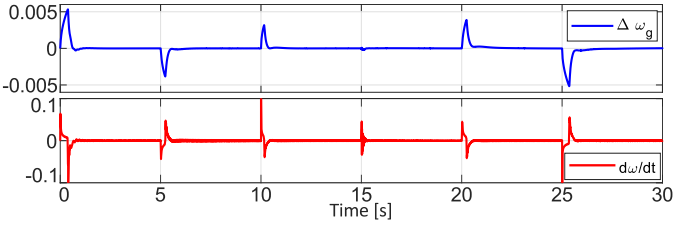

Fig. 10. The deviation of grid frequency and angular acceleration behavior.

in frequency dynamics and transient variations are analyzed to investigate the influence of the parameters on the system response. The concerned parameters are the fixed inertia constant H_o, the damping factor D_p, and the frequency-droop coefficient K_ω. Two cases are simulated: in the first case, both parameters are increased by 50% from their nominal values; in the second case, a reduction of 50% of these parameters is performed. The nominal values of the VSM parameters are presented in Table I.

Fig. 11 depicts the dynamic behavior of frequency, inertia coefficient, frequency deviation, and frequency RoCoF respectively with different parameters values, where only the strongest transient periods are shown. The nominal values (from Table I) are depicted in blue, the parameters increased by 50% in red, and the parameters decreased by 50% in black. It is clearly seen that when the parameters increase by 50% (in red), the frequency variations are considerably reduced, that is, the frequency Nadir is improved and the frequency deviation is also improved along with the frequency RoCoF. However, the speed response of frequency is slightly reduced in this case. This happens because the coefficient of inertia has greater variations during transients, acting harder to prevent frequency deviation, but also slowly reducing the frequency deviation to reach the equilibrium point. The same idea is defined for the damping coefficient. In fact as mentioned before, the adaptive virtual inertia can be interpreted as a positive damping factor added to the swing equation.

In the second case, reduced parameter values, the frequency variation increases with some oscillations appearing during transients. Frequency deviation and RoCoF also increase, since the impact of adaptive inertia is reduced. However, the convergence time is faster, which means the frequency dynamics are more sensitive to grid variations, as shown in the figure. In this way, it is possible to reach a trade off between the strength of the VSM performance for different Microgrid applications, aiming to improve inertial support. Also, the VSM parameters can be chosen regarding to grid requirements, following the limit values for frequency RoCoF and Nadir from a load change. Therefore, the operational margins of the system are fulfilled.

Another important coefficient to be explored is the constant

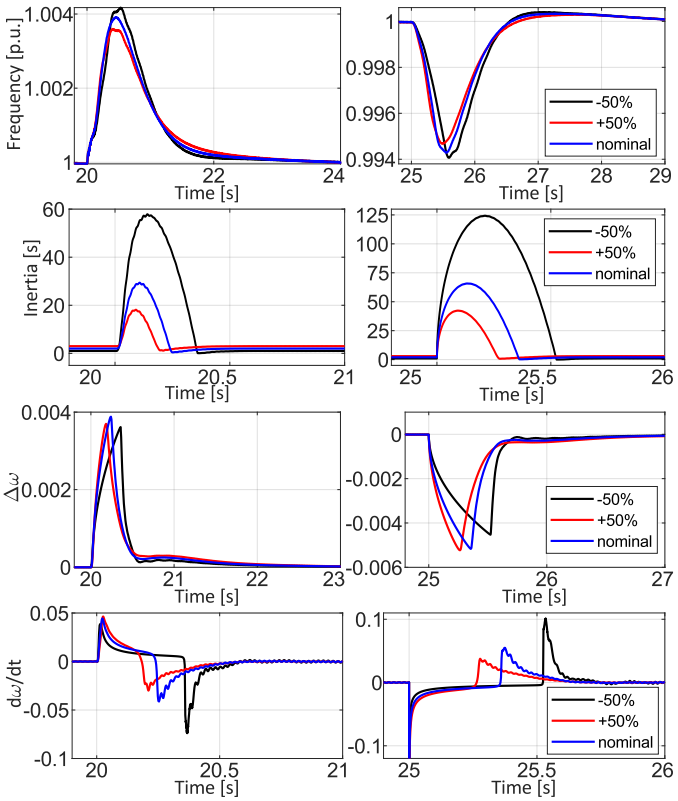

Fig. 11. Comparison among different VSM parameters considering the response of the grid frequency.

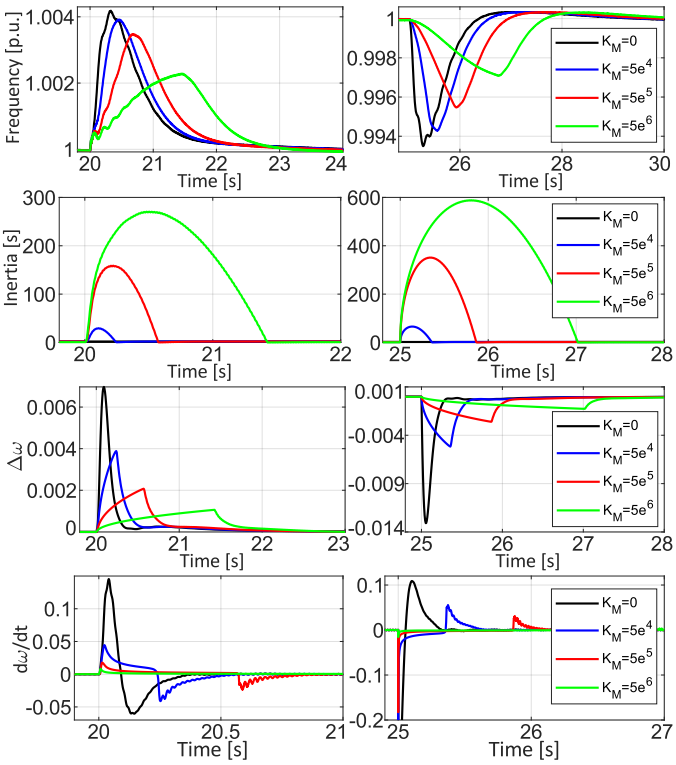

Fig. 12. The comparison of the influence on different K_M values in the adaptive inertia approach against the constant inertia case.

K_M, referring to the coefficient of adaptive inertia during transients. The adaptive inertia coefficient must be adjusted in order to obtain an improvement in the frequency response from power variations, respecting the condition in (34). Thus, different values in the constant K_M are simulated to compare the influence on frequency dynamics, including the conventional virtual inertia approach (stationary inertia coefficient $K_M = 0$).

Hereafter the following comparison is performed: how much frequency deviation and RoCoF are affected when the inertia is fixed (conventional approach) or when the adaptive inertia approach is adopted, comprising different K_M values. Four distinct scenarios are simulated: first, with constant inertia coefficient (which means $K_M = 0$); second, with $K_M = 5e{+}04$; third, with $K_M = 5e{+}05$; fourth, with $K_M = 5e{+}06$.

The comparison between the constant virtual inertia approach and adaptive virtual inertia with different K_M values is presented in Fig. 12. Initially, the frequency response of the adaptive virtual inertia is slightly slower, with smaller overshoots compared with constant inertia approach (in black), but a closer look in frequency deviation and frequency derivative shows that the constant inertia presents much larger deviations. It is clear that the value of frequency RoCoF is more than double in the conventional approach during transients. Therefore, the adaptive inertia has a great influence on frequency Nadir and RoCoF, by reducing their impacts in system operation and meeting the grid standards.

As the coefficient K_M increases, the frequency deviation decreases, improving the transient frequency response in the Microgrid, but also the speed of convergence is slightly reduced. This is clearly shown in Fig. 12, where the four scenarios are presented in detail during the largest transients. The figure presents how the moment of inertia changes according to the coefficient K_M, in particular for larger inertia coefficients, reducing frequency deviations and improving frequency Nadir and RoCoF. Also, the way in which the angular acceleration behaves in these cases is presented. It is clear that a trade off between frequency deviation and speed of convergence is needed to balance the frequency dynamics according to the Microgrid operation strategy. The insertion of a term equivalent to the angular acceleration into the inertia coefficient, reduces the frequency deviation ratio in transients.

B. Control strategy comparison

One last way to analyze the performance of the proposed control using adaptive virtual inertia is to compare it to the conventional Microgrid control strategies. To this purpose, the conventional droop control is designed in the Microgrid, the voltage droop equation is the same as in (9) and the frequency droop controller is presented as follows:

$$\omega_{droop} = \omega^* + K_p(P^* - P),$$

where the active power droop coefficient is $K_p = 0.1$. In this case, a frequency reference for the Microgrid is obtained according to power balance and the desired grid value ω^*. No dynamical effect is inserted in the droop equation for frequency support.

The second strategy carried out is the straightforward current control I_{dq}, where the power references (P^* and Q^*) are associated directly with the direct and quadrature currents as:

$$I^*_{c,d} = \frac{P^*}{V_{c,d}} \ , \ I^*_{c,q} = -\frac{Q^*}{V_{c,d}}.$$

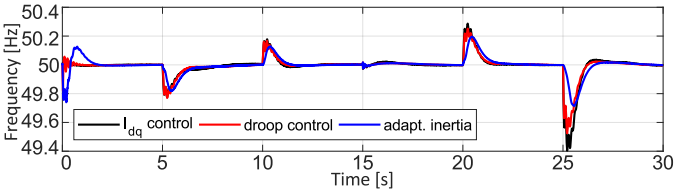

Fig. 13. A comparison among different control approaches regarding the frequency behavior.

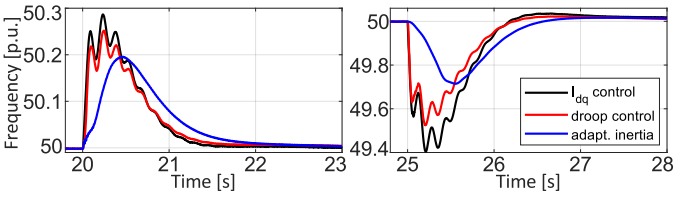

Fig. 14. A zoom of the frequency under different control strategies.

The calculated current references are applied in (43) and (44) respectively, resulting in a conventional current control strategy, without voltage control loop. The same common parameters and gains of the controllers are preserved, for comparison purposes.

The comparison among the proposed adaptive virtual inertia, the droop control, and the current control is depicted in Fig. 13, where the frequency profile is shown. A zoom presenting the strongest transient variations is introduced in Fig. 14. The droop control performs slightly better than I_{dq} current control, since droop control is able to perform power sharing while the I_{dq} control simply injects power according to its references. The convergence time is similar for the two control strategies; however the frequency deviation is evidently reduced when the adaptive virtual inertia strategy is adopted. A strong reduction in frequency oscillations during the transient is also noticed. Anyway, the major advantage of the virtual inertia strategy is the possibility to adjust the inertial parameters to obtain the proper behavior of frequency dynamics in the Microgrid, without relying on equipment physical parameters, as in the case of synchronous machines. All these elements make that the virtual inertia approach results in important advantages for Microgrids.

VI. Conclusions and Future Works

This paper proposes an overall control strategy for power converters connected to Microgrids, in the context of weak grids. One of the main features of these grids is their lack of inertia, which may lead to instability to the system for even mild disturbances. The power converters are then expected to actively participate in stabilizing the grid frequency and to provide virtual inertia and voltage support. The main original contribution of this paper especially relies on a new adaptive virtual inertia scheme, which is accordingly presented to improve inertial response of Microgrids, where inertia becomes a time-varying parameter to optimize operation and the related stability analysis solves certain critical numerical and measurement issues associated with similar solutions in the literature. The lower level voltage and current control loops are based on a nonlinear control designed to induce time-scale separation, which can explicitly include flexible protection strategies and control saturation for voltage and currents. Simulation results show the effectiveness of the proposed control strategy, where the power sharing is guaranteed when compared to other conventional approaches, with the possibility of adjusting the parameters of the VSM, such that the grid standards for frequency Nadir and RoCoF are met. Nevertheless, the analysis of the variation of parameters allows us to comprehensively evaluate their influence on the system response.

The parameters choice for inertia coefficient and damping factor is an interesting topic for future research. Optimization techniques may be applied, considering the operational margins of different power systems context as weak grids. Finally, it is worth highlighting that the case of additional converters in grid-following or grid-forming mode can be considered: the resulting control problem shall be the subject of further research efforts.

References

[1] N. Hatziargyriou, J. Milanović, C. Rahmann, V. Ajjarapu, C. Cañizares, I. Erlich, D. Hill, I. Hiskens, I. Kamwa, B. Pal *et al.*, "Stability definitions and characterization of dynamic behavior in systems with high penetration of power electronic interfaced technologies," *IEEE PES Technical Report PES-TR77*, 2020.

[2] P. F. Ribeiro, B. K. Johnson, M. L. Crow, A. Arsoy, and Y. Liu, "Energy storage systems for advanced power applications," *Proceedings of the IEEE*, vol. 89, no. 12, pp. 1744–1756, 2001.

[3] A. Arsoy, Y. Liu, and P. Ribeiro, "Static synchronous compensators and superconducting magnetic energy storage systems in controlling power system dynamics," *IEEE Industry Applications Magazine*, 2003.

[4] P. Tielens and D. Van Hertem, "The relevance of inertia in power systems," *Renewable and Sustainable Energy Reviews*, vol. 55, pp. 999–1009, 2016.

[5] W. Winter, K. Elkington, G. Bareux, and J. Kostevc, "Pushing the limits: Europe's new grid: Innovative tools to combat transmission bottlenecks and reduced inertia," *IEEE Power and Energy Magazine*, vol. 13, no. 1, pp. 60–74, 2014.

[6] F. Milano, F. Dörfler, G. Hug, D. J. Hill, and G. Verbič, "Foundations and challenges of low-inertia systems," in *2018 Power Systems Computation Conference (PSCC)*. IEEE, 2018, pp. 1–25.

[7] National Grid ESO, "Interim report into the low frequency demand disconnection (lfdd) following generator trips and frequency excursion on 9 aug 2019," in *Technical report*, 2019.

[8] E. Barklund, N. Pogaku, M. Prodanovic, C. Hernandez-Aramburo, and T. C. Green, "Energy management in autonomous microgrid using stability-constrained droop control of inverters," *IEEE Transactions on Power Electronics*, vol. 23, no. 5, pp. 2346–2352, 2008.

[9] A. Engler and N. Soultanis, "Droop control in lv-grids," in *2005 International Conference on Future Power Systems*. IEEE, 2005, pp. 6–pp.

[10] H. Han, X. Hou, J. Yang, J. Wu, M. Su, and J. M. Guerrero, "Review of power sharing control strategies for islanding operation of ac microgrids," *IEEE Transactions on Smart Grid*, vol. 7, no. 1, pp. 200–215, 2015.

[11] T. Vandoorn, J. De Kooning, B. Meersman, and L. Vandevelde, "Review of primary control strategies for islanded microgrids with power-electronic interfaces," *Renewable and Sustainable Energy Reviews*, vol. 19, pp. 613–628, 2013.

[12] Q.-C. Zhong and G. Weiss, "Synchronverters: Inverters that mimic synchronous generators," *IEEE Transactions on Industrial Electronics*, vol. 58, no. 4, pp. 1259–1267, 2010.

[13] J. Driesen and K. Visscher, "Virtual synchronous generators," in *2008 IEEE Power and Energy Society General Meeting-Conversion and Delivery of Electrical Energy in the 21st Century*. IEEE, 2008, pp. 1–3.

[14] M. Torres and L. A. Lopes, "Virtual synchronous generator control in autonomous wind-diesel power systems," in *2009 IEEE Electrical Power & Energy Conference (EPEC)*. IEEE, 2009, pp. 1–6.

[15] Y. Hirase, O. Noro, E. Yoshimura, H. Nakagawa, K. Sakimoto, and Y. Shindo, "Virtual synchronous generator control with double decoupled synchronous reference frame for single-phase inverter," *IEEJ Journal of Industry Applications*, vol. 4, no. 3, pp. 143–151, 2015.

[16] J. Alipoor, Y. Miura, and T. Ise, "Power system stabilization using virtual synchronous generator with alternating moment of inertia," *IEEE journal of Emerging and selected topics in power electronics*, vol. 3, no. 2, pp. 451–458, 2014.

[17] Y. Chen, R. Hesse, D. Turschner, and H.-P. Beck, "Improving the grid power quality using virtual synchronous machines," in *2011 international conference on power engineering, energy and electrical drives*. IEEE, 2011, pp. 1–6.

[18] T. V. Van, K. Visscher, J. Diaz, V. Karapanos, A. Woyte, M. Albu, J. Bozelie, T. Loix, and D. Federenciuc, "Virtual synchronous generator: An element of future grids," in *2010 IEEE PES Innovative Smart Grid Technologies Conference Europe (ISGT Europe)*. IEEE, 2010, pp. 1–7.

[19] S. D'Arco, J. A. Suul, and O. B. Fosso, "A virtual synchronous machine implementation for distributed control of power converters in smartgrids," *Electric Power Systems Research*, vol. 122, pp. 180–197, 2015.

[20] U. Tamrakar, D. Shrestha, M. Maharjan, B. P. Bhattarai, T. M. Hansen, and R. Tonkoski, "Virtual inertia: Current trends and future directions," *Applied Sciences*, vol. 7, no. 7, p. 654, 2017.

[21] A. W. dos Santos Serra, J. G. de Matos, L. A. de Souza Ribeiro, and L. S. Pinheiro, "Implementation of a virtual synchronous machine to improve the dynamic response of inverters," in *IECON 2019-45th Annual Conference of the IEEE Industrial Electronics Society*, vol. 1. IEEE, 2019, pp. 3912–3918.

[22] S. D'Arco, J. A. Suul, and O. B. Fosso, "Control system tuning and stability analysis of virtual synchronous machines," in *2013 IEEE Energy Conversion Congress and Exposition*. IEEE, 2013, pp. 2664–2671.

[23] K. Shi, H. Ye, W. Song, and G. Zhou, "Virtual inertia control strategy in microgrid based on virtual synchronous generator technology," *IEEE Access*, vol. 6, pp. 27 949–27 957, 2018.

[24] S. D'Arco and J. A. Suul, "Equivalence of virtual synchronous machines and frequency-droops for converter-based microgrids," *IEEE Transactions on Smart Grid*, vol. 5, no. 1, pp. 394–395, 2013.

[25] S. D'Arco, J. A. Suul, and O. B. Fosso, "Small-signal modeling and parametric sensitivity of a virtual synchronous machine in islanded operation," *International Journal of Electrical Power & Energy Systems*, vol. 72, pp. 3–15, 2015.

[26] J. Liu, Y. Miura, and T. Ise, "Comparison of dynamic characteristics between virtual synchronous generator and droop control in inverter-based distributed generators," *IEEE Transactions on Power Electronics*, vol. 31, no. 5, pp. 3600–3611, 2015.

[27] X. Hou, Y. Sun, X. Zhang, J. Lu, P. Wang, and J. M. Guerrero, "Improvement of frequency regulation in vsg-based ac microgrid via adaptive virtual inertia," *IEEE Transactions on Power Electronics*, vol. 35, no. 2, pp. 1589–1602, 2019.

[28] X. Hou, H. Han, C. Zhong, W. Yuan, M. Yi, and Y. Chen, "Improvement of transient stability in inverter-based ac microgrid via adaptive virtual inertia," in *2016 IEEE Energy Conversion Congress and Exposition (ECCE)*. IEEE, 2016, pp. 1–6.

[29] E. N. of Transmission System Operators, "Stability management in power electronics dominated systems: A prerequisite to the success of the energy transition," *ENTSO-E Position Paper*, vol. 1, p. 16, 2022.

[30] S. D'Arco and J. A. Suul, "Virtual synchronous machines—classification of implementations and analysis of equivalence to droop controllers for microgrids," in *2013 IEEE Grenoble Conference*. IEEE, 2013, pp. 1–7.

[31] F. Perez, G. Damm, F. Lamnabhi-Lagarrigue, P. F. Ribeiro, and R. Morano, "Adaptive variable synthetic inertia from a virtual synchronous machine providing ancillary services for an ac microgrid," in *IFAC World Congress 2020*. IFAC, 2020.

[32] H. A. Alsiraji and R. El-Shatshat, "Comprehensive assessment of virtual synchronous machine based voltage source converter controllers," *IET Generation, Transmission & Distribution*, vol. 11, no. 7, pp. 1762–1769, 2017.

[33] F. Perez, A. Iovine, G. Damm, L. Galai-Dol, and P. F. Ribeiro, "Stability analysis of a dc microgrid for a smart railway station integrating renewable sources," *IEEE Transactions on Control Systems Technology*, 2019.

[34] E. D. Sontag, "Input to state stability: Basic concepts and results," in *Nonlinear and optimal control theory*. Springer, 2008, pp. 163–220.

[35] K. F. Krommydas and A. T. Alexandridis, "Modular Control Design and Stability Analysis of Isolated PV-Source/Battery-Storage Distributed Generation Systems," *IEEE Journal on Emerging and Selected Topics in Circuits and Systems*, vol. 5, no. 3, pp. 372–382, Sept 2015.

[36] A. Iovine, G. Damm, E. De Santis, M. D. Di Benedetto, L. Galai-Dol, and P. Pepe, "Voltage Stabilization in a DC MicroGrid by an ISS-like Lyapunov Function implementing Droop Control," in *2018 European Control Conference (ECC)*, June 2018, pp. 1130–1135.

[37] W. Cao, M. Han, X. Meng, W. Xie, Z. W. Khan, J. M. Guerrero, and G. Agundis-Tinajero, "Reverse droop control-based smooth transfer strategy for interface converters in hybrid ac/dc distribution networks," *CSEE Journal of Power and Energy Systems*, 2020.

[38] K. De Brabandere, B. Bolsens, J. Van den Keybus, A. Woyte, J. Driesen, and R. Belmans, "A voltage and frequency droop control method for parallel inverters," *IEEE Transactions on power electronics*, vol. 22, no. 4, pp. 1107–1115, 2007.

[39] Y. A.-R. I. Mohamed and E. F. El-Saadany, "Adaptive decentralized droop controller to preserve power sharing stability of paralleled inverters in distributed generation microgrids," *IEEE Transactions on Power Electronics*, vol. 23, no. 6, pp. 2806–2816, 2008.

[40] M. Shukla and A. Sekar, "Study of the effect of x/r ratio of lines on voltage stability," in *Proceedings of the 35th Southeastern Symposium on System Theory*. IEEE, 2003.

[41] F. Welck, D. Duckwitz, and C. Gloeckler, "Influence of virtual impedance on short circuit performance of virtual synchronous machines in the 9-bus system," in *NEIS 2017; Conference on Sustainable Energy Supply and Energy Storage Systems*. VDE, 2017.

[42] O. Saborio Romano, "Small-signal modelling and stability analysis of a traditional generation unit and a virtual synchronous machine in grid-connected operation," Master's thesis, NTNU, 2015.

[43] X. Wang, Y. W. Li, F. Blaabjerg, and P. C. Loh, "Virtual-impedance-based control for voltage-source and current-source converters," *IEEE Transactions on Power Electronics*, vol. 30, no. 12, pp. 7019–7037, 2014.

[44] J. He and Y. W. Li, "Analysis, design, and implementation of virtual impedance for power electronics interfaced distributed generation," *IEEE Transactions on Industry Applications*, vol. 47, no. 6, pp. 2525–2538, 2011.

[45] N. G. Bretas and L. F. Alberto, "Lyapunov function for power systems with transfer conductances: extension of the invariance principle," *IEEE Transactions on Power Systems*, vol. 18, no. 2, pp. 769–777, 2003.

[46] P. Kundur, N. J. Balu, and M. G. Lauby, *Power system stability and control*. McGraw-hill New York, 1994, vol. 7.

[47] J. Xiao, Y. Jia, B. Jia, Z. Li, Y. Pan, and Y. Wang, "An inertial droop control based on comparisons between virtual synchronous generator and droop control in inverter-based distributed generators," *Energy Reports*, vol. 6, pp. 104–112, 2020.

[48] K. Sakimoto, Y. Miura, and T. Ise, "Stabilization of a power system with a distributed generator by a virtual synchronous generator function," in *8th International Conference on Power Electronics-ECCE Asia*. IEEE, 2011, pp. 1498–1505.

[49] J. Machowski, J. Bialek, and J. Bumby, *Power system dynamics: stability and control*. John Wiley & Sons, 2011.

[50] Y. Chen, G. Damm, A. Benchaib, M. Netto, and F. Lamnabhi-Lagarrigue, "Control induced explicit time-scale separation to attain dc voltage stability for a vsc-hvdc terminal," in *IFAC Proceedings Volumes (IFAC-PapersOnline)*, vol. 19, 08 2014.

[51] Y. Chen, W. Huang, Y. Li, H. Rao, S. Xu, and G. Damm, "Nonlinear control design for multi-terminal voltage-sourced converter high voltage direct current systems with zero dynamics regulation," in *2019 4th IEEE Workshop on the Electronic Grid (eGRID)*, 2019, pp. 1–8.

[52] Y. Chen, M. J. Carrizosa, G. Damm, F. Lamnabhi-Lagarrigue, M. Li, and Y. Li, "Control induced time-scale separation for multi-terminal high voltage direct current systems using droop control," *IEEE Transactions on Control Systems Technology*, vol. 28, no. 3, pp. 967–983, May 2020.

[53] A. Iovine, S. B. Siad, G. Damm, E. D. Santis, and M. D. D. Benedetto, "Nonlinear control of a dc microgrid for the integration of photovoltaic panels," *IEEE Transactions on Automation Science and Engineering*, vol. 14, no. 2, pp. 524–535, April 2017.

[54] F. Perez, A. Iovine, G. Damm, and P. Ribeiro, "DC microgrid voltage stability by dynamic feedback linearization," in *2018 IEEE International Conference on Industrial Technology (ICIT)*, Feb 2018, pp. 129–134.

[55] H. K. Khalil, *Nonlinear control*. Prentice Hall, 2014.

[56] C. M. Verrelli and P. Tomei, "Adaptive learning control for nonlinear systems: A single learning estimation scheme is enough?" *Automatica*, under review.

[57] D. Lee, "Ieee recommended practice for excitation system models for power system stability studies," *IEEE Std 421.5-2016*, pp. 1–207, Aug 2016.